THE PENNSYLVANIA STATE UNIVERSITY
SCHREYER HONORS COLLEGE

DEPARTMENT OF MATERIALS SCIENCE AND ENGINEERING

Electrochemical Reduction of Transition Metal Oxides in Lithium Chloride Salt at 650°C

TIMOTHY PICKARSKI
SPRING 2023

A thesis
submitted in partial fulfillment
of the requirements
for baccalaureate degrees
in Materials Science and Engineering
with honors in Materials Science and Engineering

Reviewed and approved* by the following:

Hojong Kim
Associate Professor of Materials Science and Engineering
Thesis Supervisor

Amy Robinson
Associate Teaching Professor of Materials Science and Engineering
Associate Head for Undergraduate Studies
Honors Adviser

*Signatures are on file in the Schreyer Honors College.

Abstract

The electrochemical reduction of transition metal oxides, such as iron (III) oxide (Fe_2O_3) and nickel (II) oxide (NiO), is of significant interest in various fields such as recycling and metallurgy. This study investigates the electrochemical behavior and reduction of Fe_2O_3 in a molten lithium chloride (LiCl) while outlining the design process used to efficiently create robust and effective electrodes for electrochemical testing. Supported by a range of electrochemical and subsequent characterization techniques, the main objective of this research is to gain a better understanding of the electrode design process while probing into the reduction process of these transition metal oxides in molten salt systems, paving the way for the development of more efficient and sustainable processes in relevant applications. Voltammetry and chronoamperometry were employed to study the electrochemical reduction process of Fe_2O_3 in LiCl at 650°C, though novel cavity electrode designs did not permit the examination of exact reduction peaks. The changes in the density of sintered oxide pellets were explored along with techniques to manipulate the pellets into workable cathode materials. To explore the performance of pellet electrodes after chronoamperometry, post-reduction characterization of sintered Fe_2O_3 pellets was carried out using optical and scanning electron microscopy (SEM) imaging techniques, as well as energy-dispersive X-ray spectroscopy (EDS) analysis. Examination of the morphology showed metallization of the pellet and some deterioration of the Fe pellet, while EDS analysis confirmed the presence of predominantly elemental iron. The findings presented here can be used to inform and guide future research endeavors exploring other oxides or oxide systems, contributing to the development and optimization of electrowinning processes for transition metal oxides.

Table of Contents

List of Figures

List of Tables

Acknowledgements

I would like to express my gratitude to Dr. Hojong Kim for his support throughout this project and for providing me with invaluable opportunities as an undergraduate researcher over the past two years. I am deeply grateful for my graduate mentor, Stephanie Castro Baldivieso, for her mentorship in the lab, her guidance in teaching me various techniques, her assistance with data collection, and her review of this project as it progressed. My appreciation extends to Dr. Nathan Smith for his help during the summer with iron oxide reduction experiments and for his mentorship. I am especially thankful to Dr. Amy Robinson for her role as my honors advisor, for supervising this thesis, and for her continued support. Additionally, I would like to express my gratitude for the funding I received for part of this work through the Erickson Discovery Grant over the summer of 2022. Finally, I would like to thank the PSU MatSE Department for fostering a supportive environment and for providing resources throughout my academic journey.

Chapter 1

Introduction

1.1 Motivation and Environmental Context

Traditional extraction processes for converting nickel (Ni) and iron (Fe) ores into their metallic forms are both energy and carbon-intensive. In the case of Ni, pyrometallurgical methods such as ferronickel smelting and matte smelting dominate the industry, involving multiple steps like drying, calcination, and reduction before ultimately producing metallic Ni consuming 174 GJ of energy per ton of Ni and releasing 14 tons of CO_2 [1]. Meanwhile, the primary method for producing iron, the blast furnace-basic oxygen furnace (BF-BOF) route, follows a process including sintering, coke production, and the reduction of iron ore in the blast furnace, consuming 15.7 GJ per ton of pig iron and releasing 1.9 tons of CO_2 [2]. These traditional processes have two primary factors contributing to their high carbon emissions: the elevated operating temperatures, reaching above 1500°C, which lead to increased energy consumption, and the use of carbon-based reducing agents such as coke, which release CO_2 during carbothermic reduction reactions [1, 2, 3].

As a result, there is a growing need to explore new, lower-impact approaches to metal extraction that enable lower operating temperatures and do not necessitate the use of carbon as a reductant [3]. One promising pathway for achieving this exists through the application of electrochemistry; by introducing electrons as the reductant, the process can then be made carbon-free [3, 4]. Thus, this paper primarily focuses on exploring the design process and challenges associated with electrode development in molten salt electrolysis (MSE) for the purpose of reducing transition metal oxides (TMOs), specifically nickel and iron oxide (NiO and Fe_2O_3), into their metallized forms using a molten lithium chloride (LiCl) electrolyte, highlighting the potential of this alternative approach.

1.2 Molten Salt Electrochemistry

High-temperature molten salts exhibit beneficial properties such as low viscosity for smooth flow, high diffusivity for efficient ion transport, electrochemical stability, and a wide electrochemical window for stable reduction processes with minimal side reactions [5]. Molten salts provide a suitable environment for metal extraction using MSE, offering a more sustainable and efficient approach than traditional methods [4, 5]. Specifically, LiCl electrolyte, with a melting point of 605°C, allows for operation at 650-750°C [6]. Understanding the electrochemistry of molten salts and their effects on molten salt electrolysis is crucial.

Molten salts consist of charged ions in the liquid state, enabling ion conduction through diffusion in the electrolyte [5, 7]. This mobility allows electric current flow through the molten salt, facilitating electrochemical reactions [7]. At the cathode, metal ions in the molten salt are reduced, gaining electrons and forming pure metal deposits. Conversely, oxidation reactions occur at the anode, which may involve anode material consumption or gaseous byproduct generation [5, 8].

For iron and nickel extraction using MSE, the half-reactions occurring at the cathode can be represented as follows [8]:

$$\mathrm{Fe^{3+}} + 3\,\mathrm{e^-} \longrightarrow \mathrm{Fe_{(s)}} \tag{1.1}$$

$$\mathrm{Ni^{2+}} + 2\,\mathrm{e^-} \longrightarrow \mathrm{Ni_{(s)}} \tag{1.2}$$

Indicating the reduction of the iron(III) and nickel(II) oxide to their reduced, metallic, forms. The other half reaction will occur on the anode; for reactions involving free oxygen ions in solution and the sacrificial graphite (carbon) anode used in this study, the oxidation reaction forms carbon dioxide [8]:

$$\mathrm{C_{(s)}} + 2\,\mathrm{O^{2-}} \longrightarrow \mathrm{CO_{2(g)}} + 4\,\mathrm{e^-} \tag{1.3}$$

This reaction results in the generation of CO_2 gas, which must be considered when evaluating the environmental impact of the MSE process.

In conclusion, molten salt electrolysis is a promising alternative to conventional smelting meth-

ods for extracting metals such as iron and nickel. By taking advantage of the electrochemical properties of metal oxides in molten salts, the conversion of the oxide to its reduced form is possible at temperatures significantly lower than the high melting points of the oxides. A deeper understanding of this system will allow for greater control in the development of low-temperature electrowinning techniques, giving molten salt electrolysis the potential to contribute to a more sustainable future.

1.3 Lithium-Bismuth Reference Electrode

A reference electrode plays a crucial role in electrochemical systems by providing a stable reference potential against which other electrochemical potentials can be measured. An unstable reference electrode can lead to erroneous measurements and inaccurate conclusions about the system, so a well-defined reference electrode, which maintains its potential within approximately 5 mV, is essential to obtain reliable electrochemical data. Previous work by Ning et al. employed the stable 60:40 mole ratio Li:Bi reference alloy [9]. The stability of this composition can be understood by studying the Li-Bi phase diagram shown in Figure 1.1; at 650°C, the intermetallic Li_3Bi is formed at 75 mol% Li and melts to liquid at 52 mol% [10].

In this concentration range, a mixture of the liquid and Li_3Bi is formed such that the stable exchange reaction in a 60:40 Li:Bi alloy can be described as:

$$\mathrm{Bi_{(l)}} + 3\,\mathrm{Li_{(l)}} \longleftrightarrow \mathrm{Li_3Bi_{(s)}} \tag{1.4}$$

The Li_3Bi in the electrode stabilizes the concentration of Li in the melt, maintaining the potential of the Li-Bi reference electrode across a wide range of lithium concentrations [9]. The stable exchange reaction in the alloy ensures that the reference electrode does not deplete during electrochemical measurements.

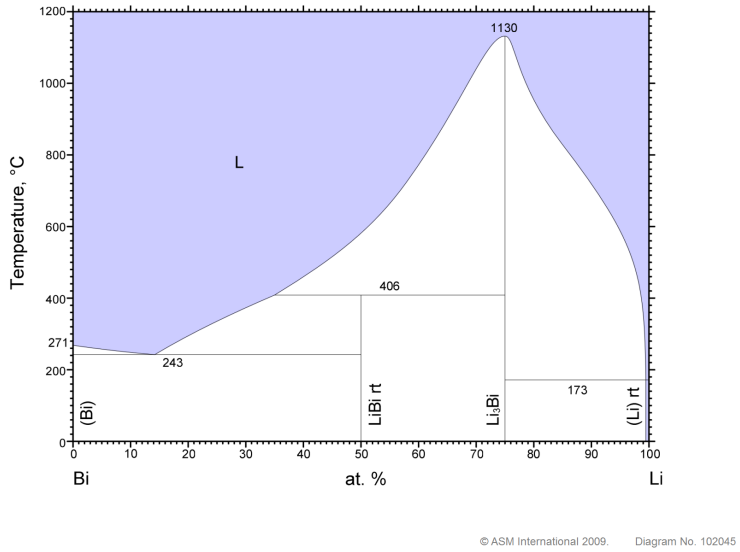

Figure 1.1: Li-Bi Phase Diagram [10]

In conclusion, the lithium-bismuth alloy reference electrode offers numerous benefits, including stability, well-defined potential, and compatibility with molten salt electrolytes such as LiCl. These characteristics make it an ideal choice for the electrowinning of NiO and Fe_2O_3. The process used to construct a reference electrode using this stable alloy is discussed in chapter 3.3.

1.4 Overview of the Electrode Development Process

The development of electrode materials in this study involved an iterative approach crucial to improving performance and stability. Electrodes needed to withstand harsh molten salt conditions, be effective, and allow for extraction and examination after testing. Establishing a consistent and repeatable process for building and rebuilding electrodes was essential. The focus was on developing cavity electrodes for voltammetry and pellet electrodes for chronoamperometry, ensuring sufficient contact between the electrolyte and wire for efficient charge transfer. Challenges encountered during design and construction were addressed through continuous improvement and optimization of fabrication techniques, discussed in chapter 3. This iterative process led to the successful development of electrode materials for the study's electrochemical experiments and the streamlined construction of reference electrodes with reliable electrochemical properties.

Chapter 2

Powder Sintering

2.1 Background

Powder sintering is a key step in preparing robust and cohesive pellets for use in electrochemical experiments involving molten salts. Sintering involves the consolidation of powdered materials, such as NiO and Fe_2O_3, into a solid mass using heat and pressure [11]. The driving force behind sintering is the reduction of surface energy, which causes particle rearrangement and grain growth within the material. During sintering, atomic diffusion occurs at the particle boundaries, allowing grains to grow and interconnect, ultimately leading to the densification of the material [11]. This results in a microstructure with strong grain-to-grain contacts, which contributes to the pellet's mechanical strength and stability, essential properties for use in molten salt electrochemical experiments. to withstand the harsh conditions and stresses experienced during electrochemical testing [11, 12, 13].

Furthermore, the densification of the material during sintering reduces the porosity of the pellet, minimizing the infiltration of molten salts into the pellet and potential dissolution of the material [12, 13]. Lastly, sintered pellets possess a uniform and interconnected grain structure, which enhances the pellet's electrical conductivity and electrochemical performance [11, 13].

This project aimed to refine and optimize the pressing and sintering processes for both small and large oxide pellets, ensuring robust and consistent pellet quality for subsequent immersion and electrochemical testing in the LiCl electrolyte. The research initially focused on the testing of small Fe_2O_3 pellets, as the process for NiO had already been established by Stephanie Castro Baldivieso. As the project progressed, the scope expanded to include the development and optimization of both

Fe_2O_3 and NiO pellets with a 10 mm diameter. The pellet preparation began with die-pressing. Unmodified oxide powder, either NiO (99%, Thermoscientific) or Fe_2O_3 (99.9%, Alfa Aesar), did not maintain its shape after pressing, necessitating the addition of a binding agent. Thus, approximately 5 g of oxide powder was mixed with 10 drops of polyvinyl-alcohol (PVA) solution, made by dissolving 1.5 g of PVA powder (Lab grade, Fisher Science Education) in 100 ml of distilled water. The powders were then left to dry in a fume hood overnight.

After drying, the modified oxide powders were pressed into pellets of two different diameters: 3.175 mm for Fe_2O_3 pellets and 10 mm for both NiO and Fe_2O_3 pellets. The pressing process involved the same steps for both small and large pellets but was optimized based on the size of the pellets.

2.2 Densification of Oxide Pellets

The pellets were then sintered in the lab sintering oven (Carbolite, BLF 1700) to ensure adequate strength for testing. First, they were heated in an initial step to 200°C to dry any atmospheric water trapped within the pellets. Next, the pellets were brought to 550°C to decompose the PVA in the pellet. The removal of the binder is essential to avoid the formation of voids or defects in the final pellet, which could compromise its structural integrity. Finally, they were brought to a final sintering temperature of 1400°C to encourage the grains of oxide to fuse together within the final pellet. Post-sintering, the pellets' height, diameter, and mass were remeasured, then used to calculate the resulting increases in density and porosity.

The porosity of the pellets were calculated using eq. 2.1:

$$Porosity(\%) = 1 - \frac{\rho_{\text{pellet}}}{\rho_{\text{bulk}}} \tag{2.1}$$

The bulk densities (ρ_{bulk}) for Fe_2O_3 and NiO are 5.25 g/cm^3 and 6.67 g/cm^3 respectively, as reported in the Sigma-Aldrich safety data sheets [14, 15].

To fabricate the 3.175 mm pellets, 30 mg of Fe_2O_3 was pressed using a dry-pressing die at 500

MPa for 10 seconds. The dimensions and mass of these pellets were measured before and after sintering. The decrease in mass and volume is summarized in Table 2.1. The standard deviation for the measurements is also provided to demonstrate uniformity in the sintering process.

	Mass (mg)	**St. Dev. (mg)**	**Volume (mm^3)**	**St. Dev. (mm^3)**
Pre-sintering	30.0	3.2	9.50	0.55
Post-sintering	29.4	4.7	6.63	0.34

Table 2.1: Mass and Volume for 3.175 mm Fe_2O_3 pellets pre- and post-sintering.

The volume decreased by 2.87 mm^3, while the mass did not decrease as much at 0.6 mg. Furthermore, the Fe_2O_3 pellets turned from a reddish-brown color to a silver color after sintering. In order to confirm no chemical changes had occurred within the sintered pellet, it was ground in a mortar and pestle; since the resulting powder was again reddish-brown, the process was not adjusted. The average densities and standard deviations of the density and porosity of the small pellets before and after sintering are shown in Table 2.2.

	ρ **(g/cm^3)**	**St. Dev. (g/cm^3)**	**Porosity (%)**	**St. Dev. (%)**
Pre-sintering	3.15	0.07	39.8	1.2
Post-sintering	4.69	0.05	10.5	0.1

Table 2.2: Pellet densities and porosities for 3.175 mm Fe_2O_3 pellets pre- and post-sintering.

The decrease in mass after sintering is attributed to the vaporization of water and PVA while the reduction in volume demonstrates grain growth and densification after sintering. This overall increase in density resulted in enhanced robustness and structural integrity, which was crucial for their subsequent immersion and electrochemical testing in the LiCl electrolyte. The small Fe_2O_3 pellets reduced in porosity from 29.3% to 10.5%, increasing its ability to perform well in testing.

The larger 10 mm pellets were created by adding 600 mg of powder to a 10 mm dry-pressing die, pressed to 187.2 MPa, held for 30 seconds, then extracted. The height, diameter, and mass of these pellets were measured. The changes in mass, volume, density, and porosity for NiO are shown in Tables 2.3 and 2.4.

	Mass (mg)	**St. Dev. (mg)**	**Volume (mm^3)**	**St. Dev. (mm^3)**
Pre-sintering	583.9	74.6	126.6	14.6
Post-sintering	574.6	76.1	106.3	10.3

Table 2.3: Mass and volume for 10 mm NiO pellets pre- and post-sintering.

	ρ **(g/cm^3)**	**St. Dev. (g/cm^3)**	**Porosity (%)**	**St. Dev. (%)**
Pre-sintering	4.62	0.11	30.8	1.2
Post-sintering	5.40	0.25	19.0	3.9

Table 2.4: Pellet densities and porosities for 10 mm NiO pellets pre- and post-sintering.

In the sintering process of NiO pellets, the initial pre-sintering density was higher in comparison to the small Fe_2O_3 pellets since NiO is denser than Fe_2O_3. However, despite the higher starting density, the densification achieved for the NiO pellets was not as significant as that observed for the Fe_2O_3 pellets. The porosity of the larger NiO pellets reduced from 30.8% to 19.0%, while the density increased from 4.62 g/cm^3 to 5.40 g/cm^3 after sintering. Although the densification was less pronounced, the sintering process still resulted in enhanced robustness and structural integrity of the NiO pellets.

The changes in mass and volume for the 10 mm Fe_2O_3 pellet are shown in Table 2.5; however, the standard deviation for the volume of the sintered pellets is high. This suggests that there was some inconsistency in the sintering process for these large Fe_2O_3 pellets.

	Mass (mg)	**St. Dev. (mg)**	**Volume (mm^3)**	**St. Dev. (mm^3)**
Pre-sintering	587.0	6.6	206.4	0.6
Post-sintering	580.8	7.4	144.0	25.4

Table 2.5: Mass and volume for 10 mm Fe_2O_3 pellets pre- and post-sintering.

The interquartile range for the post-sinter volume is between 132.94 and 134.06 mm^3. Based on this, there is a significant outlier in the data, with a volume of 195.86 mm^3. After removing the outlier, the results of sintering 10 mm Fe_2O_3 pellets are detailed in Tables 2.6 and 2.7

	Mass (mg)	**St. Dev. (mg)**	**Volume (mm^3)**	**St. Dev. (mm^3)**
Pre-sintering	587.0	6.6	206.4	0.6
Post-sintering	581.4	8.2	133.7	0.8

Table 2.6: Mass and volume for 10 mm Fe_2O_3 pellets pre- and post-sintering with outlier removed.

	ρ **(g/cm^3)**	**St. Dev. (g/cm^3)**	**Porosity (%)**	**St. Dev. (%)**
Pre-sintering	2.84	0.03	45.7	0.6
Post-sintering	4.35	0.08	17.0	1.5

Table 2.7: Pellet densities and porosities for 10 mm Fe_2O_3 pellets pre- and post-sintering with outlier removed.

The sintering of the 10 mm Fe_2O_3 pellets with the outlier removed resulted in a decrease in porosity from 45.7% to 17.0% and an increase in density from 2.84 g/cm^3 to 4.35 g/cm^3. The outlier pellet's volume could be attributed to various factors such as uneven heating within the sintering oven or slight variations in the amount of PVA binder in the pellets. Despite the inconsistency, the sintered 10 mm Fe_2O_3 pellets still showed an overall increase in density and decrease in porosity, indicating a level of densification that beneficial for further testing.

In conclusion, the sintering of Fe_2O_3 and NiO pellets resulted in increased density and decreased porosity, which are essential for their intended use in electrochemical testing. The small Fe_2O_3 pellets showed the most significant densification and uniformity in the sintering process, while the larger Fe_2O_3 and NiO pellets displayed some inconsistency in the process. Further optimization of the sintering process and investigation into potential causes for inconsistencies in the larger Fe_2O_3 pellets may be necessary. Nonetheless, the sintering process proved successful in enhancing the mechanical and structural properties of the pellets, making them suitable for immersion and electrochemical testing in the LiCl electrolyte.

Chapter 3

Electrode Development

3.1 Pellet Electrode Development

After sintering, the next step was to focus on creating reliable designs for testing in the molten salt environment. The first attempt at an electrode design using the sintered pellets involved the use of 304 stainless steel mesh baskets to hold 3.175 mm iron oxide pellets during chronoamperometry experiments. These mesh basket electrodes were created by cutting and wrapping a 2 by 1 cm rectangle of 304 stainless steel mesh around a sintered 3.175 mm Fe_2O_3 pellet. After forming a square around the pellet, it was spot-welded closed then to a cleaned 45 cm long, 1.2 mm diameter Fe (99+%, Alfa Aesar) wire with the end flattened using the U.S. Solid USS-BSW00004 spot welder. The main challenge in this process was attaching the flag to the wire while maintaining stability. Spot welding required two hands, so the wire had to be secured to the lab bench using tape, with the flattened end parallel to the working surface.

However, the mesh basket electrodes exhibited significant degradation after chronoamperometry, making it difficult to extract the iron pellets. Figure 3.1 shows a side-by-side comparison of the mesh basket electrode before and after exposure to the molten salt environment, with the clean mesh shown in 3.1a and the degraded mesh shown in 3.1b.

Thus, a new pellet electrode design was needed that maintained electrochemical contact without the mesh. Stephanie Castro Baldivieso introduced the concept of drilling a hole through a pellet and mounting it to a wire. The next development was the process to drill 1.0 or 1.5 mm holes into the brittle pellets. Holes were introduced both pre- and post-sintering. Pre-sintering drilling was easier but introduced stress into the pellet, potentially causing it to break during sintering.

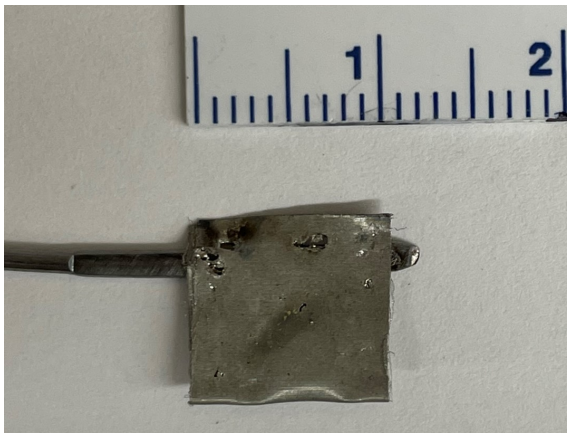

(a) Clean mesh basket electrode

(b) Degraded mesh basket electrode

Figure 3.1: Comparison of the mesh basket electrode before (a) and after (b) chronoamperometry.

Consequently, a post-sintering hole drilling process was developed, focusing on NiO pellets. Drilling through the pellets was initially done by hand, holding the drill bit stationary while pushing down and spinning the pellet on a paper towel. This process was time-consuming and labor-intensive. To speed up the process, a method was developed to hold the small 1mm drill bit in the lab drill. The end of the 1 mm drill bit was wrapped tightly in painter's tape, and the tape was compressed in a vice to eliminate any flexibility, allowing the lab drill to grip the bit while staying centered. The lab drill could grip the 1.5 mm bit, so it was used as normal to bore through the pellets. This more aggressive drilling process required caution, as the heavy drill could fracture the pellet if too much pressure was applied or if the operator's hand twisted. The final drilling process was faster, but care was needed to avoid applying excessive force. For Fe_2O_3 pellets, which responded better to sintering with pre-drilled holes, both hand-held bits and the drill were viable options. Hand-held bits were slower but more reliable, while the drill was faster but more prone to damaging the pellet.

3.2 Cavity Electrode Development

The initial design, introduced by Dr. Nathan Smith, was developed for use in Fe_2O_3 reduction experiments. This design consisted of a clean Fe wire with a flattened end and an approximately

1 mm dimple pressed into it. Green iron oxide powder was loaded into the dimple and pressed to secure it. However, during electrochemical testing, the iron oxide too easily fell out of the cavity due to insufficient friction between the metal and the oxide, especially considering the careful handling needed during the cell construction process. The subsequent iteration consisted of a small stainless steel cylinder (1 cm long, 3.5 mm diameter) with a 1.5 mm hole bored into the side, packed with the Fe_2O_3. This design held the Fe_2O_3 more effectively compared to the dimpled wire but did not yield good results after electrochemical testing.

Inspired by Qiu et al.'s development of metallic cavity electrodes for investigating powders in molten $CaCl_2$, the next design was developed in collaboration with Stephanie Castro Baldivieso. This study used molybdenum foil with mechanically drilled holes of 1 mm or laser beam cut holes of 0.3-0.5 mm [16]. For this design, both 1.2 mm Fe and Ni (99.5%, Alfa Aesar) wires were first cleaned using sandpaper and then wiped down with a paper towel and isopropyl alcohol (IPA). Next, a 1.5 cm section of wire was flattened then sent to the machine shop to drill 1.5 mm holes into the flattened end. The oxides were pressed into the hole for use in electrochemical experiments. 3.2 shows two of the current cavity electrode designs. Wires with the same metal species as the oxide were used. The challenge with this design was the 1.5 mm hole size; to decrease the current density at the cathode, future work should focus on strategies to create smaller holes for the cavity electrodes.

Figure 3.2: Current Cavity Electrode Design (Fe wires)

3.3 Reference Electrode Development

For accurate potential measurements, the Li-Bi alloy at x_{Li} = 0.60 in a boron nitride (BN) crucible served as the reference electrode. The BN crucible was fabricated by first cutting a 3 cm section of 2 cm diameter BN feedstock (Momentive). The BN cylinder was inserted into the laboratory lathe (Central Machinery, 7" x 10" Precision Mini Lathe), and the ends were flattened and sanded smooth. First, a 5 mm diameter pilot hole was drilled 2 cm into the crucible to remove the majority of the material, then a 7.85 mm diameter flat bottom hole was drilled 2.5 cm into the cylinder using a flat drill bit. Finally, two 1 mm cavities were drilled through the crucible 7 mm above the bottom of the crucible. The completed crucibles were sonicated in IPA and left to dry in a drying oven overnight at 135°C.

In order to fabricate the Li-Bi alloy, approximately 2.85763g of Bi (99.999%, Sigma Aldrich) and 0.142369g of Li were weighed out under an argon atmosphere. The Bi was melted in a stainless steel tray on a hot plate, and the Li was slowly added in pieces to the Bi melt. The development process of the stainless steel tray involved addressing the issues of warping and Li-Bi melt containment. Initial attempts involved cutting an approximately 3 by 4 cm section of stainless steel shim, then bending the sides up using pliers to create a lip the melt could not escape from. This approach had one problem: as the tray heated, the strained shim could warp, causing the Li-Bi melt to be ejected from the tray. To solve this issue, an approach to reduce the amount of bending on the steel's base was employed. First, relief cuts were made in the corners of the shim before bending, so there was no folding metal. Eventually, larger trays were used, which had a lower tendency to warp during the heating process. Once the tray issue was resolved, the alloy was allowed to cool, cut into pieces, and poured into a prepared BN cylinder. The filled crucible was introduced to an induction heater installed inside the glovebox under an inert argon atmosphere and heated until the alloy was completely remelted. A clean 45 cm long tungsten (W) (0.98 mm, 99.95%, Thermo Shield) wire was lowered into the melted alloy and the completed reference electrode was allowed to cool completely and stored under argon.

Chapter 4

Experimental

4.1 Electrochemical cell components

4.1.1 Electrolyte Preparation

The LiCl electrolyte was prepared by taking an appropriate amount of ultra-dry LiCl (99.9%, Alfa Aesar) powder, which was poured into an alumina crucible (AdValue Technology) then transferred to a stainless-steel vacuum chamber for drying. The chamber was inserted into a crucible furnace and heated under vacuum at various temperatures to dry the salt mixture. The chamber was then purged with ultra-high purity argon (Ar) gas and heated to 100°C for 8 hours, followed by 270°C for 8 hours, and finally 450°C for 8 hours. After cooling, the dry LiCl electrolyte was ground into a fine powder using a mortar and pestle for use in the electrochemical cell.

4.1.2 Three-Electrode Setup

The electrochemical testing employed a three-electrode setup, consisting of a working electrode, a counter electrode, and a reference electrode. Details on the construction process and challenges are provided in Chapter 3. This setup was utilized for all the electrochemical testing designs, additional electrodes employed that did not require an iterative design process were, clean W, Fe, and Ni wires for calibration.

Lastly, a graphite counter electrode was prepared to maintain a stable current flow in the cell and balance the charge. To fabricate this, a 50 cm long, 3 mm diameter threaded stainless steel rod was cleaned with a paper towel and isopropyl alcohol. A 2 cm long section of 1 cm diameter

graphite rod was prepared and attached to the laboratory lathe. A 2.5 mm diameter hole was drilled 1.5 cm into the graphite cylinder, which was then threaded to allow the stainless steel rod to be screwed on.

The three-electrode electrochemical cell configuration is shown in Figure 4.1.

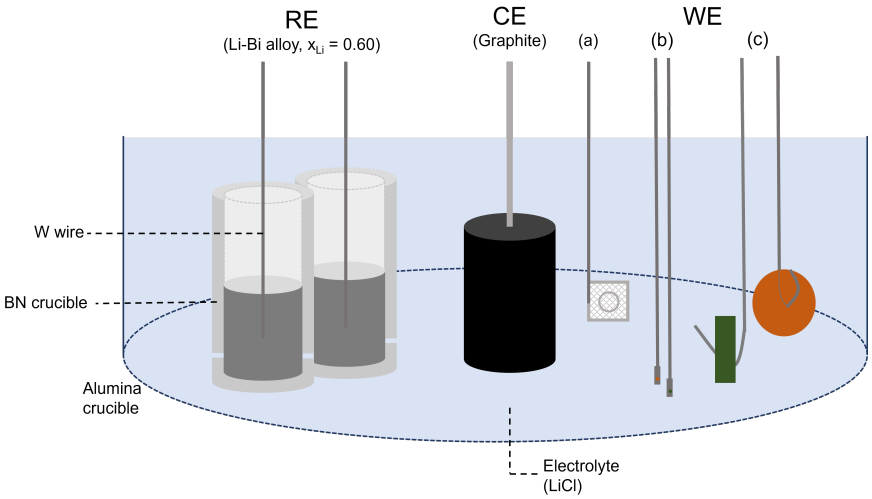

Figure 4.1: Three-electrode electrochemical cell diagram

The various working electrode designs are designated as follows: (a) for the mesh basket, (b) for the cavity electrodes, and (c) for the pellet electrodes, shown for both oxides, red representing Fe_2O_3 and green representing NiO.

4.1.3 Cell Assembly

The cell assembly process took place inside an Ar-filled glovebox (O_2 concentration $<$0.5 ppm). First, the graphite cylinder was removed from the steel rod, which was then sheathed in a single-bore alumina tube (Advalue Technology) and placed into the testing chamber, after which the graphite cylinder was reattached. Two single-bore alumina tubes were inserted into the testing chamber, and two reference electrodes were guided through the tubes until their tungsten leads were visible at the top of the chamber. This process was also used for both pellet and mesh basket electrodes. For cavity or blank electrodes, these smaller components were inserted into double-bore alumina tubes (Advalue Technology) and dropped directly into the test chamber.

An alumina crucible (250 mL, Advalue Technology) was then positioned within the test chamber and the electrodes were placed inside the crucible. The two reference electrodes were lowered to rest on the bottom of the crucible, while the counter electrode was set to float 1 cm above the crucible's base. The working electrodes were held at a higher position. Electrodes in single-bore alumina tubes were sealed with epoxy, while the double-bore alumina tubes provided a snug enough fit to eliminate the need for epoxy. The salt was poured into the filled crucible, the test chamber was sealed inside a glovebox, loaded into a furnace, and evacuated to approximately 1 Pa. The crucible was then heated to 650°C under flowing Ar. Throughout the electrochemical testing, the working electrode being tested was lowered into the molten salt for its test and raised back up upon completion.

4.2 Electrochemical Techiques

The transition metal oxides' behavior was characterized using controlled-potential electrochemical techniques. An electrochemical reduction proceeds according to the half-reaction:

$$\mathrm{O^+ + ne^- \longrightarrow R} \qquad \mathrm{E^o = E_{rxn}} \tag{4.1}$$

Which is associated with the oxidized species O^+, a reduced species R, and some reduction potential E_{rxn} [8]. When a voltage more cathodic than E_{rxn} is applied, reduction of the oxidized species will occur through electron transfer, inducing a current recorded in the NOVA software. Constant and differential potential techniques were employed in this study. The reduction potential(s) of each oxide system were examined using the differential voltage techniques of cyclic voltammetry (CV) and linear sweep voltammetry (LSV). These measure the current response versus the potential of the system for linear potential vs. time functions.

4.2.1 Cyclic and Linear Sweep Voltammetry

The prepared electrochemical cell was heated to 650°C to melt the LiCl electrolyte, with two reference electrodes submerged in the electrolyte. A voltammeter was used to measure the potential difference between the reference electrodes to ensure their stability. Once confirmed, the working electrode of interest was connected to the potentiostat (Metrohm, Autolab PGSTAT302N) along with the counter and reference electrodes.

The system was allowed to stabilize to its open circuit potential (OCP), then a triangular voltage waveform was applied to the working electrode and the resulting current-potential curve (voltammogram) was recorded.

For linear sweep voltammetry measurements, a linear voltage waveform was applied to the working electrode, sweeping from a positive (anodic) potential to a negative (cathodic) potential. The resulting voltammograms were recorded and examined. Following the voltammetry tests, the electrodes were subjected to chronoamperometry.

4.2.2 Chronoamperometry

Chronoamperometry is a technique used to study electrode behavior when held at a constant potential for a defined period. In this research, reducing potentials found from voltammetry measurements were applied to the working electrodes and the resulting current was measured over time. Faraday's Law, a fundamental principle in electrochemistry, governs the relationship between charge, chemical change, and time [8]. During experiments, a constant potential was applied to the working electrode containing oxide pellets, and the current as a function of time was monitored. As the TMO's reduction proceeded, the current changed in response to the chemical transformation at the electrode surface. After tests were completed, electrodes were raised out of the electrolyte and the cell was cooled to room temperature for extraction and examination.

4.3 Electrode Characterization

Upon completing the electrochemical experiments, a thorough characterization of the reduced pellets was carried out using Scanning Electron Microscopy - Energy Dispersive Spectroscopy (SEM-EDS). The characterization process involved several steps, beginning with the extraction of the electrodes. First, the electrochemical cell was allowed to cool down to room temperature, ensuring the safe handling and extraction of the electrodes. Once at a safe temperature, the pellets were carefully recovered from the cell and prepared for further analysis. To facilitate a comprehensive examination of the pellet's internal structure, each pellet was cut vertically in half using a low-speed diamond saw. This cut exposed the interior of the electrodes, allowing for analysis of their morphology and composition.

Next, the working electrode (WE) half of the pellet was securely mounted in epoxy, providing a stable base for the subsequent polishing process. To achieve a smooth and uniform surface, the mounted electrode was polished to a 1600 grit finish using silicon carbide paper and isopropyl alcohol. This step was crucial in ensuring the accuracy of the SEM-EDS analysis, as a properly polished surface minimizes artifacts and facilitates accurate data collection. With the sample preparation complete, the electrode halves were taken for characterization using a Scanning Electron Microscope (SEM, FEI Quanta 200) equipped with an Energy Dispersive Spectrometer (EDS). The SEM analysis allowed for a detailed examination of the electrode's morphology, highlighting changes in the microstructure as a result of the reduction process. Concurrently, the EDS analysis provided essential information on the elemental composition of the electrode. By following these steps, the electrode characterization process yielded valuable insights into the physical and chemical changes that occurred during the reduction experiment.

Chapter 5

Results and Discussion

5.1 Overview

The electrochemical reduction of transition metal oxides, specifically Fe_2O_3, was studied using various electrochemical techniques and further characterized through the analysis of the reduced electrodes. The reduction process was investigated employing linear sweep voltammetry (LSV) techniques and chronoamperometry, which were complemented by morphological and compositional analyses of the reduced pellets. In this study, the successful electrochemical reduction of Fe_2O_3 using the molten salt electrolyte, LiCl, was demonstrated to evaluate the performance of the electrode designs. The discussion of the electrode performance in testing is organized into four main sections: (1) stability of the reference electrodes, (2) evaluation of the linear sweep voltammetry data, and (3) morphological and compositional analysis of the reduced pellets.

During testing, the reference electrodes were checked for stability with respect to each other using a voltmeter. Although no specific data is available, the stability between the reference electrodes was confirmed before each measurement, ensuring the reliability of the measurements.

5.2 Linear Sweep Voltammetry Measurements

The linear sweep voltammetry measurements were performed to identify the reduction potential of Fe_2O_3. Figure 5.1 shows the voltammogram for Fe_2O_3 taken by Stephanie Castro Baldivieso using the cavity electrode design. The cavity electrode, however, did not produce defined peaks corresponding to any reduction potentials.

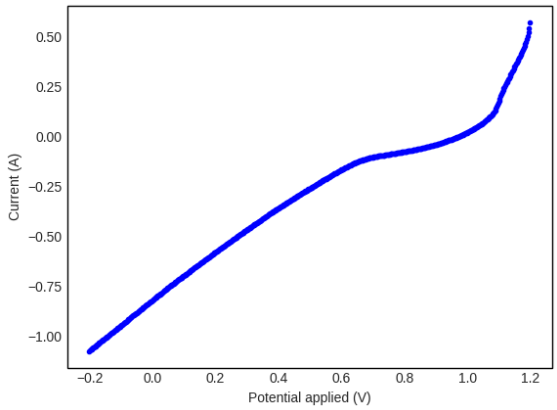

Figure 5.1: Linear voltammogram of Fe_2O_3.
Experimental data was generated by Stephanie Castro Baldivieso.

The reduction curve for Fe_2O_3 is broad, making it difficult to pinpoint a specific potential vs. Li:Bi 60:40 where the transition occurs. The current response showed a downward trend with decreasing potential. The lack of defined peaks points to issues with the electrode, such as poor contact between the electrode and the sample or large current densities from the 1.5 mm hole.

It is important to highlight that based on these voltammetry measurements, the potential for chronoamperometric measurements of Fe_2O_3 was chosen as -0.3 V vs. Li:Bi. Though the data collected by Stephanie Castro Baldivieso does not directly pertain to the physical performance of the pellet electrodes, it is worth noting chronoamperometry was employed to reduce the transition metal oxide pellets.

5.3 Morphological and Compositional Analysis

The morphological and compositional analysis of the reduced Fe_2O_3 pellet, including the optical and SEM-EDS images taken by Stephanie Castro Baldivieso, provided valuable insights into the reduction process. The reduced Fe_2O_3 pellet showed a successful reduction to its metallic form. The optical images in Figure 5.2a show the physical appearance of the reduced Fe_2O_3 pellet. The Fe_2O_3 pellet appears to be significantly reduced, but the testing seems to have degraded its physical structure.

The SEM images (Figure 5.2b) further emphasize the differences in morphology between the

reduced Fe_2O_3 pellets. The Fe_2O_3 pellet exhibits a crumbly texture. EDS analysis of the reduced Fe_2O_3 pellet (Figure 5.2c) confirms the presence of elemental iron with bright coloration in the Fe section.

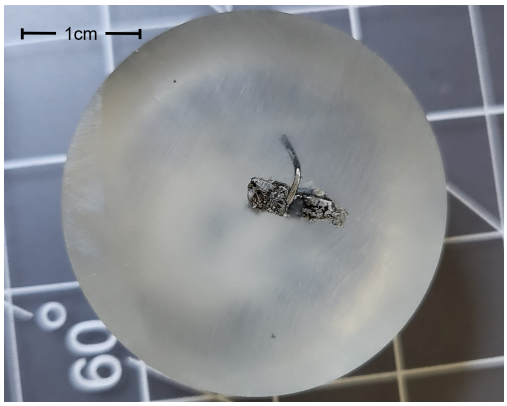

(a) Optical Image of Reduced Fe_2O_3 Pellet.

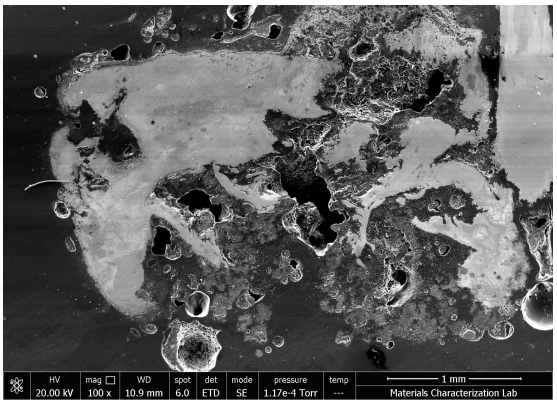

(b) SEM Image of Reduced Fe_2O_3 Pellet.

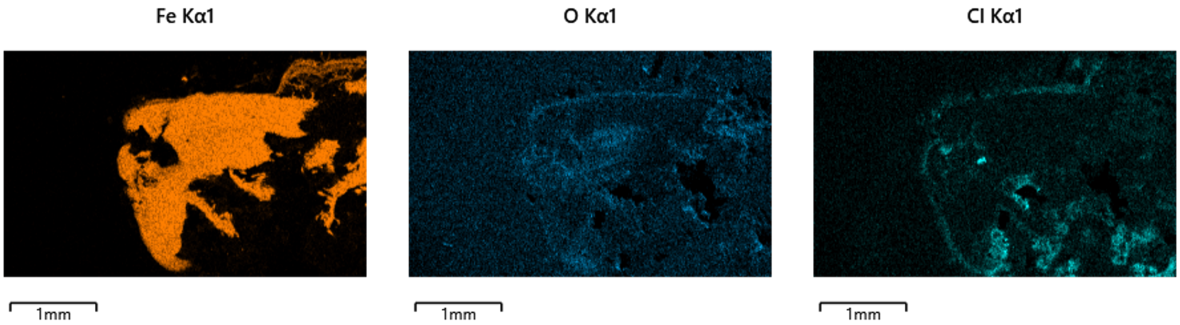

(c) EDS Analysis of Reduced Fe_2O_3 Pellet.

Figure 5.2: Optical, SEM, and EDS analysis of the reduced Fe_2O_3 pellet, showing (a) the physical appearance of the reduced pellet, (b) the differences in its morphology, and (c) the presence of elemental iron.
Experimental data was generated by Stephanie Castro Baldivieso.

Some oxygen is lightly speckled across the surface of the iron, indicating that the reduction may not have been 100% complete. Analysis of the reduced Fe_2O_3 pellet shows successful reduction of the TMO into its metallic form. However, the reduction process led to a significant degradation in the physical structure of the Fe_2O_3 pellet. The relative degradation of the iron pellet could be a cause for concern regarding the potential for the pellet to break off during testing, though the electrode ultimately withstood the testing. The EDS analysis further confirms the presence of elemental iron in the pellet.

Chapter 6

Conclusion and Future Work

In this study, the design process regarding the efficient construction of multiple different electrode types was explored through their conceptualization, preparation, construction, and analysis of their performance in electrochemical testing using the Fe_2O_3 reduction experiment. Pressing and sintering to turn green transition metal oxide powder into robust sintered pellets were shown to effectively increase the density and decrease the porosity of oxide pellets, the improvements in their mechanical strength essential to both electrochemical testing and their ease of handling in the laboratory environment. Cavity electrode designs for use in cyclic and linear sweep voltammetry measurements were explored, though limitations in hole sizing led to a lack of definitive electrochemical readings of the reduction potentials of Fe_2O_3 in molten LiCl. Future work in this area will focus on further iteration of the cavity design to ensure measurements which yield defined peaks by decreasing the diameter of the cavity.

Despite the challenges in their performance under voltammetry measurements, the Fe_2O_3 pellets withstood chronoamperometric testing and were successfully reduced to their metallic form. However, the optical and SEM images revealed that the Fe_2O_3 pellet was significantly reduced but showed signs of degradation in its physical structure. Based on the observations from the electrochemical experiments and the morphological and compositional analysis of the reduced Fe_2O_3 pellet, it appears that further work is required to improve the electrode design and achieve more accurate reduction potential measurements for the system. Additionally, alternative methods for chronoamperometry could be explored that do not require sintering a pellet, potentially reducing energy use and simplifying the experimental procedure. This would allow for a more accessible

and sustainable approach to studying the reduction of transition metal oxides. In summary, this study provided essential information regarding the reduction of Fe_2O_3 in molten LiCl as well as the design process to efficiently create electrodes for molten salt electrolysis experiments. The knowledge gained can serve as a foundation for future research and advancements in the field of electrowinning and its related applications.

Bibliography

[1] W. Wenjing, P. Samuelsson, A. Tilliander, R. Gyllenram, and P. Jönsson. Energy consumption and greenhouse gas emissions of nickel products. *Energies*, 13(21), 2020.

[2] H.Y. Sohn. Energy consumption and CO_2 emissions in ironmaking and development of a novel flash technology. *Metals*, 10(1):54, 2019.

[3] G. Li, D. Wang, and G. Chen. Direct reduction of solid Fe_2O_3 in molten $CaCl_2$ by potentially green process. *Journal of Materials Science and Technology -Shenyang-*, 25:767–771, 11 2009.

[4] D. Sadoway. New opportunities for metals extraction and waste treatment by electrochemical processing in molten salts. *Journal of Materials Research*, 10(3):487–492, 1995.

[5] Y. Yong and D. Fray. Molten salt electrolysis for sustainable metals extraction and materials processing a review. *Electrolysis: Theory, Types and Applications*, 01 2010.

[6] H. Sub Ji, H. Yeol Ryu, E.Y. Choi, S.W. Cho, M. Simpson, and S.M. Jeong. Preparation of $NdNi_5$ using an electrochemical reduction of a NiO-Nd_2O_3 mixture in molten LiCl. *Journal of Industrial and Engineering Chemistry*, 24:259–265, 2015.

[7] M.M. Walz and D. Van Der Spoel. Microscopic origins of conductivity in molten salts unraveled by computer simulations. *Communications Chemistry*, 4(1), 2021.

[8] E. McCafferty. *Introduction to Corrosion Science*. Springer New York, 2010.

[9] X. Ning, S. Phadke, B. Chung, H. Yin, P. Burke, and D. Sadoway. Self-healing Li-Bi liquid metal battery for grid-scale energy storage. *Journal of Power Sources*, 275:370–376, 2015.

[10] H. Okamoto and O. Kubaschewski. *Phase Diagrams for Binary Alloys, Desk Handbook*. ASM International, 2010.

[11] S.J.L. Kang. *Sintering: Densification, Grain Growth and Microstructure*. Elsevier Science, 2004.

[12] Y. Iida. Sintering of high-purity nickel oxide. *Journal of the American Ceramic Society*, 41(10):397–406, 1958.

[13] H.E.N. Stone. Electrical conductivity and sintering in iron oxides at high temperatures. *Journal of Materials Science*, 3(3):321–325, 1968.

[14] Sigma-Aldrich. *Iron(III) oxide, MSDS No. 529311*, 4 2023. (accessed April 7, 2023).

[15] Sigma-Aldrich. *Nickel(II) oxide, MSDS No. 481793*, 4 2023. (accessed April 7, 2023).

[16] G. Qiu, M. Ma, D. Wang, X. Jin, X. Hu, and G. Z. Chen. Metallic cavity electrodes for investigation of powders. *Journal of The Electrochemical Society*, 152(10):E328, 2005.

Timothy Pickarski

ACADEMIC VITA

EXPERIENCE

Kim Group Undergraduate Electrochemical Researcher **9/2021-Present**
Steidle Building, State College, PA

- Conducted research project on reducing conditions of Transition Metal Oxide Powders in LiCl Molten Salt by using pellet sintering, electrode fabrication, cell preparation, and linear sweep voltammetry.
- Performed cyclic voltammetry tests, electron impedance spectroscopy measurements, and SEM analysis of Nd-Bi intermetallic compounds for rare earth recycling research.

Material Science/Metallurgical Engineering Co-op **1/2021-7/2021**
Bayer Crop Science LLC, Creve Coeur, MO

- Diagnosed corrosive conditions in the Bayer Cotton Seed Fluid Bed Dryer piping failure, tested alloy behavior using High-Temperature Electrochemical testing and on-line monitoring coupon analysis, and generated a Materials of Construction recommendation report improving plant longevity.
- Integrated Bayer databases with the Knovel CorSur database to increase access to research and data of different materials' corrosion performance in varying industrial conditions.

EDUCATION

Bachelor of Science in Materials Science and Engineering **8/2019-Present**
The Pennsylvania State University Schreyer Honors College, University Park, PA

Dean's List

TECHNICAL SKILLS

Electrochemistry: Cyclic Voltammetry, Chronoamperometry, Electron Impedance Spectroscopy, Li-ion Battery Theory, Electrochemical Cell Design, Li-Bi Reference Electrode Fabrication.

Computer Skills: Advantageous experience in Python, MATLAB, and JavaScript.

Report Preparation: Basic skill with Overleaf syntax and report preparation, Experience writing Formal/Informal Lab Reports, Research Posters, White Papers, and Professional PowerPoint Presentations.

Data Analysis: One-Sample t, Binomial, Chi-Square, and ANOVA testing.

Characterization: X-ray diffraction, IR Spectroscopy, SEM/EDS, Optical Microscopy, and Physical Analysis.

EXTRACURRICULAR ACTIVITIES

Science Olympiad Alumni at Penn State, *Director of Marketing* **8/2021-Present**

- Procured funding from local businesses to buy supplies to run the Penn State Science Olympiad Invitational.
- Designed and organized the purchase of club merchandise.

Materials Advantage, *Social Chair* **5/2022-Present**
Central PA MMA Muay Thai Club, *Yellow Armband* **3/2022-Present**

HONORS AND ORGANIZATIONS

Penn State University Provost's Award **1/2019**
Erickson Discovery Grant **3/2022**
Tau Beta Pi (Engineering Honor Society) **4/2022**